Journal of the Korean Crystal Growth and Crystal Technology
Vol. 19, No. 4 (2009) 172-183

Effects of thermal boundary conditions and microgravity environments on physical vapor transport of Hg_2Cl_2-Xe system

Geug-Tae Kim†, Moo Hyun Kwon* and Kyong-Hwan Lee**

Department of Nano-Bio Chemical Engineering, Hannam University, Taejon 305-811, Korea
**Department of Applied Chemistry, Woosuk University, Wanju 565-701, Korea*
***Climate Change Technology Research Division, Korea Institute of Energy Research, Taeejon 305-343, Korea*

(Received April 20, 2009)
(Revised August 7, 2009)
(Accepted August 13, 2009)

Abstract For the effects of the nonlinear temperature profiles and reduced-gravity conditions we conduct a two-dimensional numerical modeling and simulations on the physical vapor transport processes of Hg_2Cl_2-Xe system in the horizontal orientation position. Our results reveal that: (1) A decrease in aspect ratio from 5 to 2 leads to an increasingly nonuniform interfacial distribution and enhances the growth rate by one-order magnitude for normal gravity and linear wall temperature conditions. (2) Increasing the molecular weight of component B, Xenon results in a reduction in the effect of solutal convection. (3) The effect of aspect ratio affects the interfacial growth rates significantly under normal gravity condition rather than under reduced gravitational environments. (4) The transition from the convection-dominated regime to the diffusion-dominated regime ranges arises near at $0.1g_0$ for operation conditions under consideration in this study.

Key words Mercurous chloride, Convection, Xenon, Microgravity, Physical vapor transport

1. Introduction

Physical vapor transport (PVT) has become an important crystal growth process for a variety of acousto-optic materials. The mechanism of the PVT process is simple: sublimation-condensation in closed silica glass ampoules in temperature gradient imposed between the source material and the growing crystal. It also requires minimal process control and monitoring, and transport results are easily interpreted. Of particular importance is the use of PVT for materials processing experiments in low and high gravity environments, which would provide a better and thorough understanding of transport phenomena occurring in the vapor phase and crystal growth phenomena.

Over the past 25 years many theoretical modeling studies [1-12] on transport phenomena in PVT and much quantitative experiments [13-20] have been extensively investigated. Most important theoretical works were achieved by Rosenberger [1-4, 6, 8] and, recently extended for transition to chaos flow fields in specialty materials of mercurous chloride in applications of microgravity experiments by Duval [21-25]. They have addressed the underlying phenomena in the PVT processes on the relative importance and influencing parameters of diffusion-advection, thermal and/or solutal convection on mass transport. Our recent studies [26-33] are for PVT processes of specialty materials such as mercurous halides (Hg_2Cl_2 and Hg_2Br_2) under normal and microgravity environments to investigate the role of convection on the mass transport rate and its transition from diffusion-dominated to circulatory convection-dominated regimes in relation to total pressure, temperatures of source and crystal ends, aspect ratio (transport length-to-width), molecular weights, wall temperature profiles.

It is the purpose of this paper to study systematically the transport phenomena covering the various gravity accelerations in the PVT processes of Hg_2Cl_2 crystal growth system. For this theoretical analysis of the PVT processes, a two-dimensional model is in horizontally oriented, cylindrical, closed ampoules in a two-zone furnace system. Diffusion-limited processes are considered in this paper, although Singh, Mazelsky and Glicksman [34] demonstrated that the interface kinetics plays an important role in the PVT system of Hg_2Cl_2. The effects of normal and high gravity accelerations on solutally and/or thermally buoyancy-driven convection will be considered at this point, primarily for a mixture of Hg_2Cl_2 vapor and impurity of Xenon (Xe), although for gaining insights into the convection, the low gravity environments are more important than high gravity conditions in some cases.

†Corresponding author
Tel: +82-42-629-8837
Fax: +82-42-629-8835
E-mail: gtkim@hnu.kr

2. Model and Numerical Analysis

Mercurous chloride (Hg_2Cl_2) materials are important for applications in acousto-optic and opto-electronic devices such as Bragg cells, X-ray detectors operating at ambient temperature [35]. The equimolar Hg_2Cl_2 compound decomposes to two liquids at a temperature near 525°C where the vapor pressure is above 20 atm [36, 37]. Because of this decomposition and high vapor pressure, Hg_2Cl_2 cannot be solidified as a single crystal directly from the stoichiometric melt. However, very similar to the mercurous bromide, mercurous chloride exhibits sufficiently high vapor pressure at low temperatures so that these crystals are usually grown by the physical vapor transport (PVT) in closed silica glass ampoules.

Consider a rectangular enclosure of height H and transport length L, shown in Fig. 1. The source is maintained at a temperature T_s, while the growing crystal is at a temperature T_c, with $T_s > T_c$. PVT of the transported component A (Hg_2Cl_2) occurs inevitably, due to presence of impurities, with the presence of a component B (Xe). The interfaces are assumed to be flat for simplicity. The finite normal velocities at the interfaces can be expressed by Stefan flow deduced from the one-dimensional diffusion-limited model [38], which would provide the coupling between the fluid dynamics and species calculations. On the other hand, the tangential component of the mass average velocity of the vapor at the interfaces vanishes. Thermodynamic equilibria are assumed at the interfaces so that the mass fractions at the interfaces are kept constant at $\omega_{A,s}$ and $\omega_{A,c}$. On the vertical non-reacting walls appropriate velocity boundary conditions are no-slip, the normal concentration gradients are zero, and wall temperatures are imposed as nonlinear temperature gradients. Thermo-physical properties of the fluid are assumed to be constant, except for the density. When the Boussinesq approximation is invoked, density is assumed constant except the buoyancy body force term. The density is assumed to be a function of both temperature and concentration. The ideal gas law and Dalton's law of partial pressures are used. Viscous energy dissipation and the Soret-Dufour (thermo-diffusion) effects can be neglected, as their contributions remain relatively insignificant for the conditions encountered in our PVT crystal growth processes. The transport of fluid within a rectangular PVT crystal growth reactor is governed by a system of elliptic, coupled conservation equations for mass (continuity), momentum, energy and species (diffusion). They can be represented by Eqs. (1) through (7) [39] with their appropriate boundary conditions Eqs. (8) through (10). Let u_x, u_y denote the velocity components along the x- and y-coordinates in the x, y rectangular coordinate, and let T, ω_A, p denote the temperature, mass fraction of species A (Hg_2Cl_2) and pressure, respectively, where the superscript of * denotes the dimensionless [26-33].

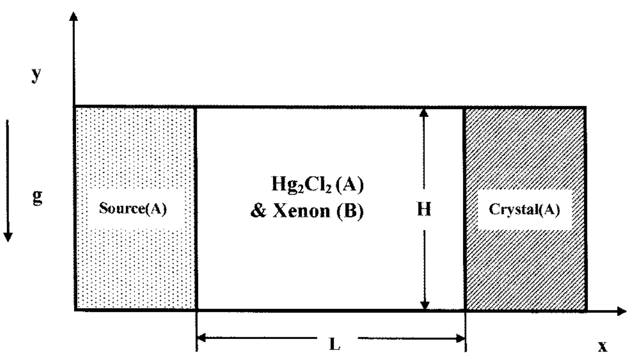

Fig. 1. Definition sketch for two-dimensional PVT model of Hg_2Cl_2-Xe system.

The dimensionless variables are defined as follows:

$$x^* = \frac{x}{H},\quad y^* = \frac{y}{H}, \tag{1}$$

$$u^* = \frac{u_x}{U_c},\quad v^* = \frac{u_y}{U_c},\quad p^* = \frac{p}{\rho_c U_c^2}, \tag{2}$$

$$T^* = \frac{T - T_c}{T_s - T_c},\quad \omega_A^* = \frac{\omega_A - \omega_{A,c}}{\omega_{A,s} - \omega_{A,c}}. \tag{3}$$

The dimensionless governing equations are given by:

$$\nabla^* \bullet \vec{V}^* = 0, \tag{4}$$

$$\vec{V}^* \bullet \nabla^* \vec{V}^* = -\nabla^* p^* + Pr \cdot Ar \nabla^{*2} \vec{V}^* - \frac{Ra \cdot Pr}{Ar} \cdot T^* \cdot e_g, \tag{5}$$

$$\vec{V}^* \bullet \nabla^* T^* = Ar \nabla^{*2} T^* \tag{6}$$

$$\vec{V}^* \bullet \nabla^* \omega_A^* = \frac{Ar}{Le} \nabla^{*2} \omega_A^* \tag{7}$$

On the walls ($0 < x^* < L/H$, $y^* = 0$ and 1):

$$u^*(x^*,0) = u^*(x^*,1) = v^*(x^*,0) = v^*(x^*,1) = 0 \tag{8}$$

$$\frac{\partial \omega_A^*(x^*,0)}{\partial y^*} = \frac{\partial \omega_A^*(x^*,1)}{\partial y^*} = 0,$$

$$T^*(x^*,0) = T^*(x^*,1) = \frac{T - T_c}{T_s - T_c}$$

On the source ($x^* = 0$, $0 < y^* < 1$):

$$u^*(0,y^*) = -\frac{1}{Le(1-\omega_{A,s})} \frac{\Delta\omega}{} \frac{\partial \omega_A^*(0,y^*)}{\partial x^*}, \tag{9}$$

$$v^*(0,y^*) = 0,$$
$$T^*(0,y^*) = 1,$$
$$\omega_A^*(0,y^*) = 1.$$

On the crystal ($x^* = L/H$, $0 < y^* < 1$):

$$u^*(L/H,y^*) = -\frac{1}{Le}\frac{\Delta\omega}{(1-\omega_{A,c})}\frac{\partial\omega_A^*(L/H,y^*)}{\partial x^*}, \quad (9)$$
$$v^*(L/H,y^*) = 0,$$
$$T^*(L/H,y^*) = 0,$$
$$\omega_A^*(L/H,y^*) = 0.$$

The crystal growth rate V_c [7, 26-33] can be expressed as follows:

$$\int\rho_v\vec{v}_v\cdot\vec{n}dA = \int\rho_c\vec{v}_c\cdot\vec{n}dA, \quad (11)$$

$$V_c = \frac{\rho_v\int\vec{v}_v\cdot\vec{n}dA}{\rho_c\int dA}. \quad (12)$$

It should be noted that from a mass balance at the crystal vapor interface, assuming fast kinetics, i.e. all the vapor is incorporated into the crystal, see refs. [26, 27] in details.

There is only limited information available for the thermophysical properties of Hg_2Cl_2, with the exception of the vapor pressure. To estimate the properties of the mixture of Hg_2Cl_2 and Xe the Chapman-Enskog relations [43] based on the Lennard-Jones potentials are used. The vapor pressure p_A of Hg_2Cl_2 was estimated from the correlation [10]

$$p_A = e^{(a-b/T)}, \quad (13)$$

in which p_A is in Pascal units, and $a = 29.75$ and $b = 11767.1$.

The detailed numerical schemes in order to solve the discretization equations for the system of nonlinear, coupled governing partial differential equations are found in ref. [42]. From considerations of both spatial convergence and accuracy, a grid mesh 23 × 43 has been found satisfactory. In each calculation, depending upon the operating conditions such as the imposed boundary conditions and the molecular weights, it takes about 5,000~10,000 iterations to reach convergence.

3. Results and Discussion

The purposes for this study is to investigate the effects of solutal convection (called as a concentration buoyancy driven convection) with gravitational acceleration and nonlinear/linear temperature profiles on the growth rate and its interfacial distributions, and the convective intensities during physical vapor transport. Because the molecular weight of a noble element xenon (Xe) is not equal to that of the crystal component (Hg_2Cl_2) during the physical vapor transport, solutal effects should be considered mainly in this study. Typical dimensionless parameters and physical properties for the operating

Table 1
Typical thermo-physical properties used in this study ($M_A = 472.086$, $M_B = 131.3$)

Transport length, L	10 cm
Height, H	2 cm
Source temperature, T_s	612.5 K
Crystal temperature, T_c	576.0 K
Thermal diffusivity, κ	0.16 cm^2/s
Kinematic viscosity, μ	0.13 cm^2/s
Diffusivity, D_{AB}	0.49 cm^2/s
Thermal expansion coefficient, β	0.0016 K^{-1}
Prandtl number, Pr	0.82
Lewis number, Le	0.33
Peclet, Pe	3.74
Concentration number, Cv	1.02
Total system pressure, P_T	293.54 Torr
Partial pressure of component B, P_B	10 Torr
Thermal Grashof number, Gr_t	2.65×10^4
Solutal Grashof number, Gr_s	2.99×10^5

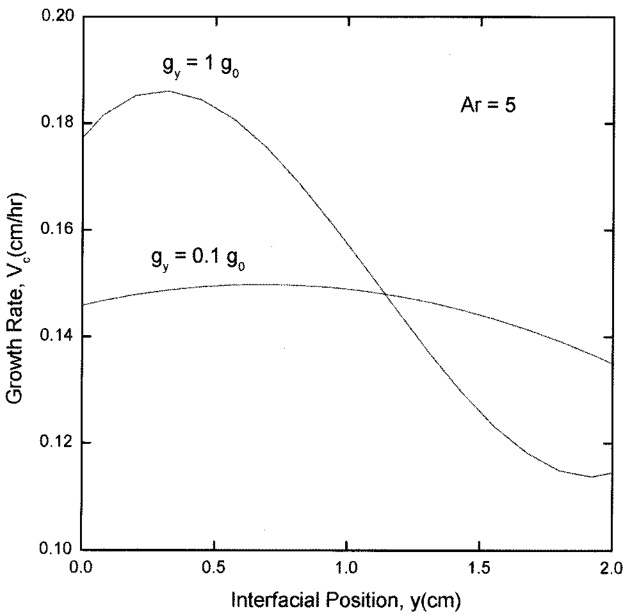

Fig. 2. Interfacial distribution of crystal growth rates for a horizontal ampoule of aspect ratio 5, a linear wall temperature profile between $T_s = 612.5$ K and $T_c = 576.0$ K, and $g_y = 1g_0$ and $0.1g_0$. Based on Ar = 5, Pr = 0.80, Le = 0.37, $Gr_t = 2.85 \times 10^4$, $Gr_s = 3.05 \times 10^5$, Pe = 2.27, $C_v = 1.11$.

conditions of this study are shown in Table 1 on the basis of Fig. 9 with the nonlinear wall temperatures.

Fig. 2 shows our results for a horizontal system of aspect ratio of 5 (L = 10 cm, H = 2 cm), with the source temperature, $T_s = 612.5$ K and the crystal temperature, $T_c = 576.0$ K, and gravity accelerations of $g_y = 1g_0$ and $0.1g_0$ in the negative y-direction, where g_0 denotes the standard terrestrial gravitational acceleration 981 cm s^{-2}. Interfacial distributions of the growth rate, indicative of nonuniformities, exhibits the effects of solutal convection. In this study thermally buoyancy driven convection (normally called as thermal convection) could be neglected because the solutal convection is one order of magnitude larger than the thermal convection. As shown

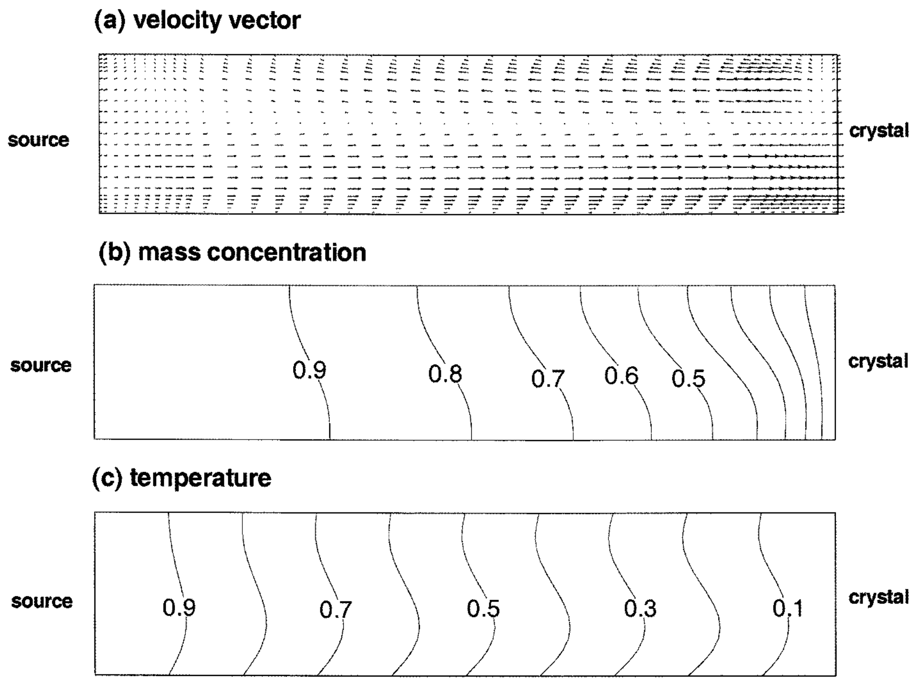

Fig. 3. Dimensionless velocity vector fields, temperature and mass concentration contours corresponding to the case of $g_y = 1g_0$ in Fig. 2. The maximum magnitude of the velocity vector is 0.45 cm s^{-1}.

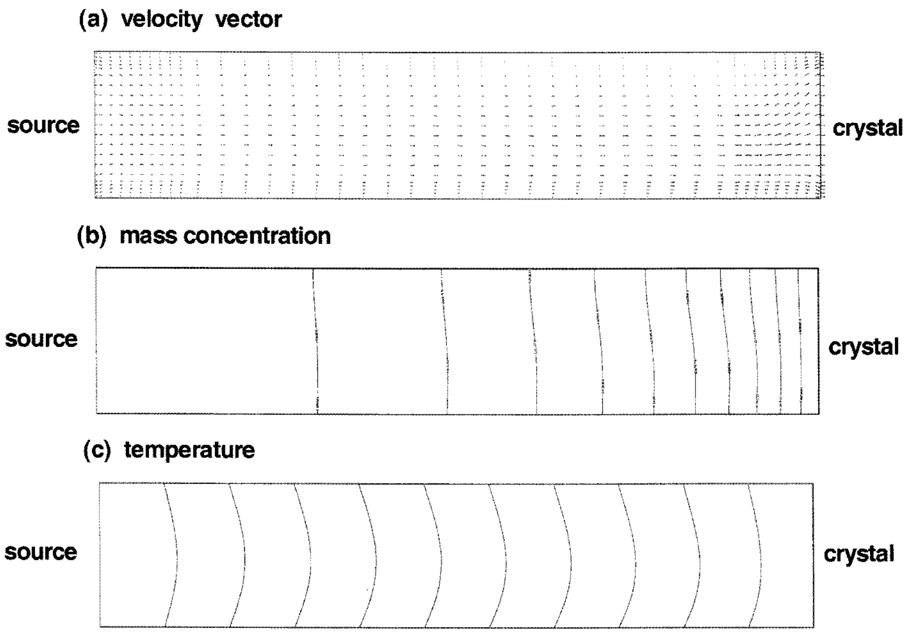

Fig. 4. Dimensionless velocity vector fields, temperature and mass concentration contours corresponding to the case of $g_y = 0.1g_0$ in Fig. 2. The maximum magnitude of the velocity vector is 0.12 cm s^{-1}.

in Fig. 2, the convection enhances the overall mass transport of component A (Hg_2Cl_2), and, then results in an increase in its growth rate, but pays for the expense of uniformity in the growth rate. Figs. 3 and 4 show dimensionless velocity vector fields, temperature and mass concentration contours corresponding to the case of $g_y = 1g_0$ and $g_y = 0.1g_0$ in Fig. 2, respectively. In Figs. 3 and 4, the maximum magnitude of the velocity vector is 0.45 cm s^{-1}, 0.12 cm s^{-1}, respectively. For the cases of $g_y = 1g_0$ and $0.1g_0$, the same governing parameters of Ar, Pe, Pr, Le and C_v are considered except for a Grashof numbers of 2.85×10^4 and 2.85×10^3, respectively. As shown in Fig. 3, the flow field shows an asymmetrical unicellular flow structure. It can be seen that no secondary flow is predicted in the neighborhood of the crystal interface. The mass concentration contours show a sharp gradient in front of the crystal interface. The temperature contours show symmetrical at y = 1 and are in well linearly ordered arrangement. This reflects the importance of solutal convection rather than thermal convection for PVT operating conditions under consideration. As can be seen in Fig. 4, the dimensionless velocity vector field shows relatively asymmetrical uniflow profiles with velocities at bottom walls greater than at top walls. The corresponding mass concentration and temperature contours are symmetrical. It can be found that no cellular convective flow structure appears in the vapor phase during the PVT processes under $0.1g_0$. Therefore, the reduction in solutally buoyancy-induced convection results in improved uniformity of growth at the crystal interface. In other words, the recirculating flow have a significant effect on the distribution of growth rate at the crystal interface. The differences in flow fields obtained between under normal and one tenth-reduced gravitational environments are attributed to the effects of gravity on the vapor phase transport mechanism. Also, the transition from recirculating flow due to solutal buoyancy convection to diffusion-dominant mode is reflected in the interfacial velocity. Note diffusion-dominant mode is not necessarily attained in buoyancy-free environments under PVT processes with thermal creep phenomena [41].

Fig. 5 shows the results for a system with an aspect ratio 2 (L = 4 cm), $T_s = 612.5$ K and $T_c = 576.0$ K, the gravity accelerations of $g_y = 1g_0$ and $0.1g_0$, $g_x = 1g_0$ and $0.1g_0$, where $g_y = 1g_0$ and $g_x = 1g_0$ correspond to the horizontal and the vertical orientations against the gravity vector, respectively. Note Figs. 2 and 5 are based on $P_B = 50$ Torr, and linear wall temperature profiles. As can be seen in Figs. 2 and 5, the rates for Ar = 2 are

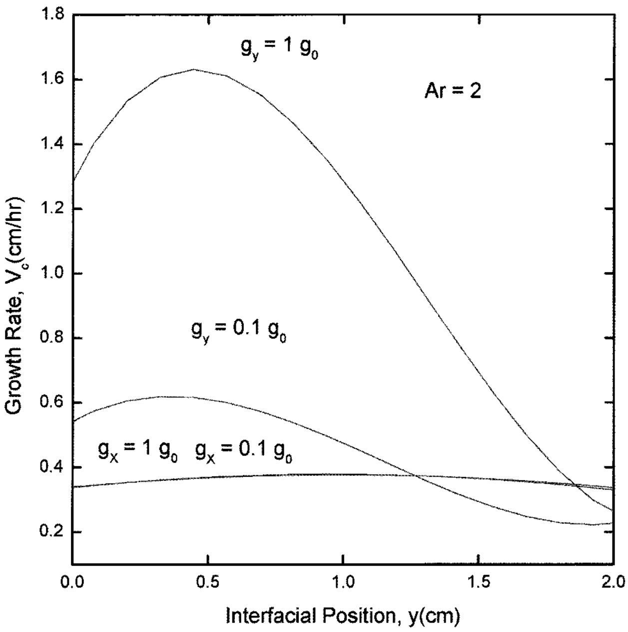

Fig. 5. Interfacial distribution of crystal growth rates for a horizontal ampoule of aspect ratio 2, a linear wall temperature profile between $T_s = 612.5$ K and $T_c = 576.0$ K, and $g_y = 1g_0$ and $0.1g_0$. Based on Ar = 2, Pr = 0.86, Le = 0.23, $Gr_t = 2.14 \times 10^4$, $Gr_s = 2.78 \times 10^5$, Pe = 2.74, $C_v = 1.07$.

much greater than for Ar = 5 as well as the nonuniformities in interfacial distributions because of the effects of convection. The maximum rates for both Ar = 2 and 5 occur in the neighborhood of interfacial position, y = 0.5 cm. For Ar = 2, the reduction in gravitational level from $g_y = 1g_0$ to $0.1g_0$ in the horizontal orientation position weakens the effect of convection significantly. For example, the maximum rate of 1.61 cm/hr at $g_y = 1g_0$ is reduced to 0.61 cm/hr. It is clear that a factor of ten reduction in the gravitational level is enough to suppress the convective effects on the growth rate. In reduced gravity environments the growth rates can be also controlled by altering the aspect ratio of ampoules, i.e., the smaller the aspect ratio is, the larger the growth rate is, under otherwise unchanged operating conditions. Under normal gravitational conditions, as the aspect ratio is reduced from 5 down to 2, i.e., by a factor of 0.4, the maximum rate for Ar = 2 is found to be one order of magnitude larger than for Ar = 5. On the other hand, under one tenth-reduced gravitational conditions, the former is four times greater than for the latter. Under reduced-gravity environments a factor of 0.4 reduction in an aspect ratio enhances the maximum rate by a factor of 4. As can be seen in Fig. 5, the convection under the horizontal orientation affects more significantly the growth rate than under the vertical orientation. It should be emphasized that the buoyancy driven convection due to density gradients always occurs in the horizontal orientation. For the system under consideration in this study solutally buoyancy driven convection is much more dominant by one order magnitude than thermally buoyancy driven convection. The growth rate in the vertical orientation with the bottom-heated source, top-positioned crystal (referred as thermally convective-destabilizing orientation) is nearly invariant with the gravity levels of both $g_x = 1g_0$ and $0.1g_0$. This indicates the mass transport is mainly governed by the diffusion rather convection mode, at least, in the vertical orientation under consideration in this study. The diffusive effects are reflected through governing parameters of Lewis and Peclet number. As seen in Figs. 2 and 5, small non-uniformities in the growth rates appear even in the ten reduction of gravitation level, which is likely to stem from the recirculation of the inert gas. It is consistent with the results of [1] which addressed, the nonuniformity can occur even for the condition of zero gravity. Note even for purely diffusive transport the growth rate is not strictly uniform, with growth being greater near the center than near the walls. In addition, the pattern of the interfacial distribution for $Ar = 2$ is more axisymmetrical against $y = 0.5$ than for $Ar = 5$, which reflects the competition between the intensity of convection and the effects of side walls [26, 42, 43].

Fig. 6 shows the influence of molecular weight M_B on interfacial distribution of crystal growth rates for a horizontal ampoule of aspect ratio 5, with a linear wall temperature profile between $T_s = 612.5$ K and $T_c = 576.0$ K, $g_y = 1g_0$, $4 \leq M_B \leq 472$. As the molecular weight of component B, Xenon increases from 2 up to 472, i.e. closer to that of the growing mercurous chloride crystals, the effect of solutal convection decreases, which is indicative of the transition from convection-dominated mode to diffusion-dominated. Also, increasing of the inert gas with the molecular weight M_B could enhance the intensity of thermal convection in comparison with solutal convection, i.e., thermal convection becomes much dominant in the convection mode. To be specific, as the $M_B \rightarrow M_A$ (= 472 g/gmole), the rate for $M_B = 2$ is reduced to the rate for $M_A = 472$ by a factor of ten reduction in the rate, which implies the solutal convection-dominated regime is switched over the thermal regime. Note thermally buoyancy driven convection only is governed when the molecular weights of A and B are equal, in other words thermal convection overcomes solutal convection. The density dependence on the solute and temperature can be expressed by the following Boussinesq approximation:

$$\rho = \rho_0(1 - \beta\Delta T + \gamma\Delta\varpi), \quad (14)$$

where β is a thermal volume expansion coefficient and γ is a pressure-dependence coefficient. It can be well

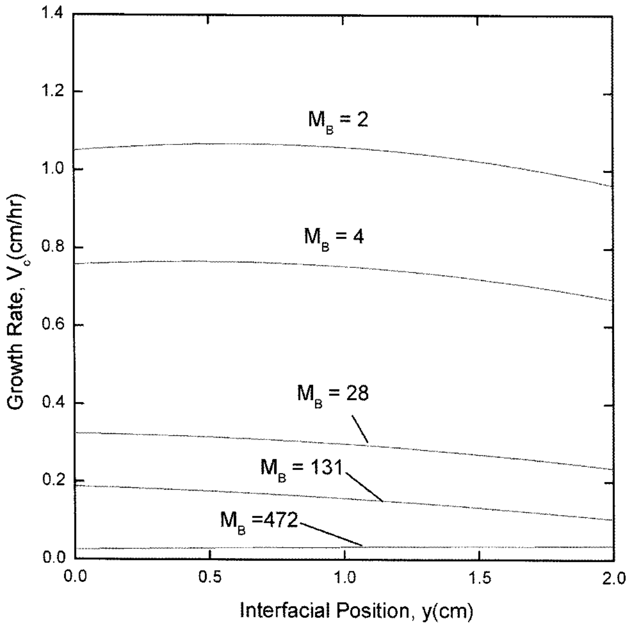

Fig. 6. Influence of molecular weight M_B on interfacial distribution of crystal growth rates for a horizontal ampoule of aspect ratio 5, with a linear wall temperature profile between $T_s = 612.5$ K and $T_c = 576.0$ K, $g_y = 1g_0$, $4 \leq M_B \leq 472$.

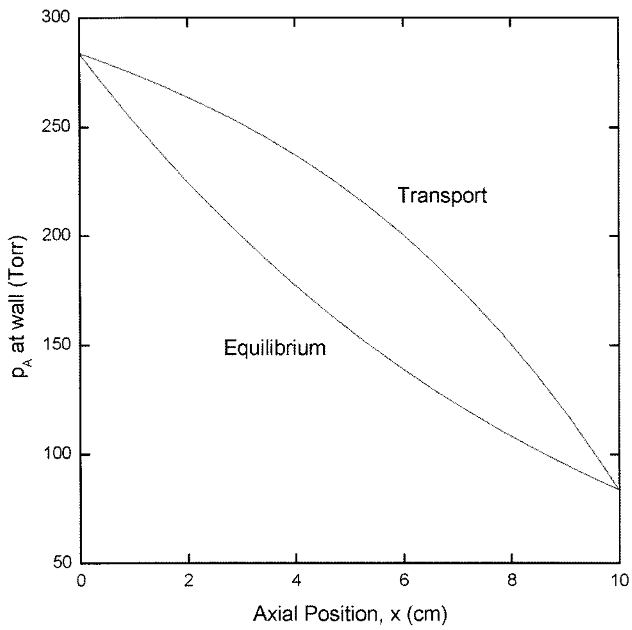

Fig. 7. Axial distribution of partial pressure of component A at the walls resulting from purely diffusive transport for $Ar = 5$ and the linear wall temperature profile between $T_s = 612.5$ K and $T_c = 576.0$ K. The equilibrium vapor pressure profile corresponding to the wall temperature distribution is shown for the purpose of comparison. Based on $Ar = 5.0$, $Pr = 0.8$, $Le = 0.37$, $Gr_t = 0$, $Gr_s = 0$, $Pe = 2.27$, $Cv = 1.1$, $g_y = 0$.

understood from Eq. (14) the situations of thermal convection only caused by the interactions between the thermal density gradient and the gravity acceleration.

Fig. 7 shows the axial distribution of partial pressure of component A at the walls resulting from purely diffusive transport for Ar = 5, the linear wall temperature profile between $T_s = 612.5$ K and $T_c = 576.0$ K, and $M_B = 131.3$ g/gmole. Also, the equilibrium vapor pressure profile corresponding to the wall temperature distribution is shown for the purpose of comparison. The equilibrium vapor pressures of component A at the wall temperatures are calculated from Eq. (13). The partial pressures of component A at the walls are obtained from purely diffusive transport phenomena. Fig. 7 are based on Ar = 5.0, Pr = 0.8, Le = 0.37, $Gr_t = 0$, $Gr_s = 0$, Pe = 2.27, Cv = 1.1, and $g_y = 0$. Fig. 8 shows the axial distribution of partial pressure of component A at the walls resulting from diffusive-convective transport at $g_y = 1g_0$, with the same system as for Fig. 7 except with $Gr_t = 2.8 \times 10^4$, $Gr_s = 3.05 \times 10^5$, $g_y = 1g_0$. As shown in Figs. 7 and 8, the pressures of Hg_2Cl_2 (component A) vapors in the top and the bottom walls are above the corresponding equilibrium pressures so that the vapors of are in a supersaturated state throughout the vapor phase in the ampoule. Such a vapor supersaturation could cause undesirable parasitic nucleations at the walls and, thus in actual experiments a linear wall temperature condition is not employed frequently [6].

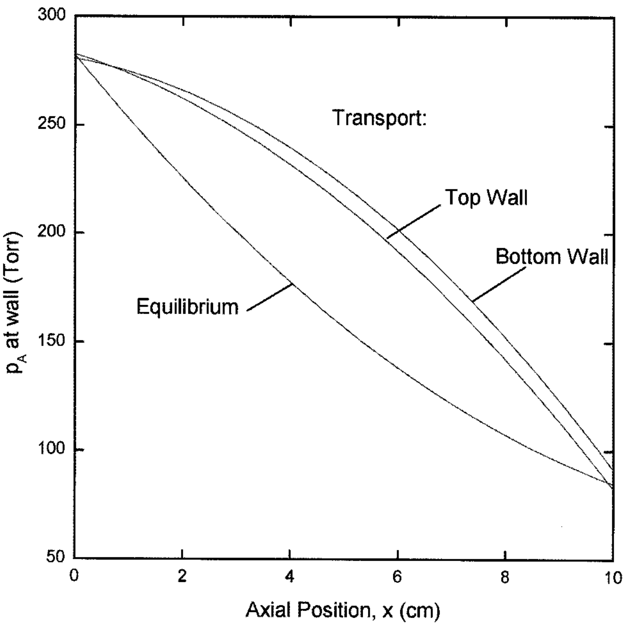

Fig. 8. Axial distribution of partial pressure of component A at the walls resulting from diffusive-convective transport at $1g_y = 1g_0$, and equilibrium vapor pressure for Ar = 5 and linear wall temperature profile between $T_s = 612.5$ K and $T_c = 576.0$ K. Based on Ar = 5.0, Pr = 0.8, Le = 0.37, $Gr_t = 2.8 \times 10^4$, $Gr_s = 3.05 \times 10^5$, Pe = 2.27, Cv = 1.11, $g_y = 1g_0$.

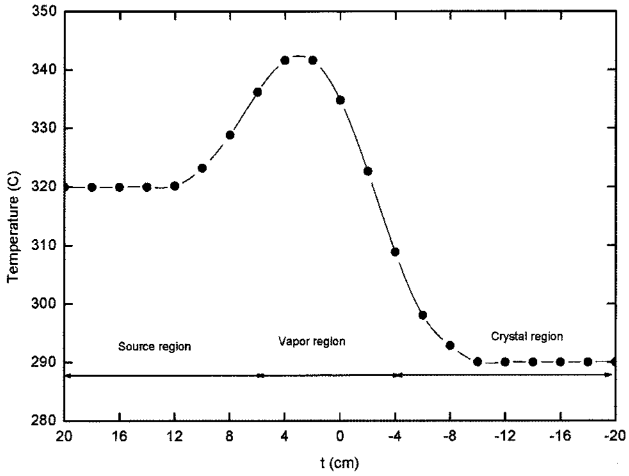

Fig. 9. The nonlinear temperature profile along the ampoule [11].

As shown in Fig. 9, such a hump region corresponding to the location of the vapor component A and B inside the ampoule is used in actual experiments to avoid parasitic nucleations at the walls resulting from the supersaturations along the transport path. The following temperature profile was used as a boundary condition along the ampoule (y = 0 and y = H): this equation [11] is expressed in reference to an approximate fit of experimental data, see Fig. 9.

$$T(t) = \begin{cases} 563.16 & \text{for } -20 \le t \le -10\text{cm} \\ 608 + 4.97t - 0.70t^2 \\ -5.91\times10^{-2}t^3 + 6.67 & \text{for } -10 \le t \le 12\text{cm} \\ \times10^{-3}t^4 + 2.60\times10^{-4}t^5 \\ -2.49\times10^{-5}t^6 \\ 593.16 & \text{for } 12 \le t \le 20\text{cm} \end{cases} \quad (15)$$

During the crystal growth the ampoule is placed in the nonlinear thermal profile as shown in Fig. 9. The hump region corresponds to the location of the vapor component A and B inside the ampoule. The source material lies in the region with the larger temperature near $t \ge 8$ cm. Whereas crystal growth occurs in the region corresponding to $t \le -4$ cm. In the experiments one positions the ampoule in the growth region with a temperature less than the source in order to drive the process. In addition, the length of the hump region can also be adjusted so that we have a much larger source region. With respect to Fig. 9, the following transformation is used to relate the laboratory reference to the ampoule: where K_i is the position of the source and vapor inter-

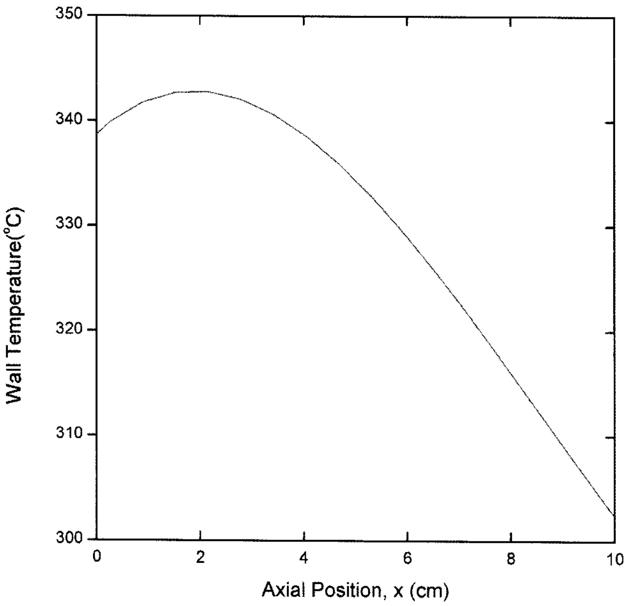

Fig. 10. A nonlinear axial wall temperature profile given by Eq. (5) with maximum ("hump") for Ar = 5, T_s = 612.5 K and T_c = 576.0 K.

face in the laboratory reference frame.

Fig. 10 shows an axially nonlinear wall temperature profile given by Eq. (15) with maximum ("hump") for Ar = 5, T_s = 612.5 K and T_c = 576.0 K. Because the aspect ratio of 5 with L = 10 cm and H = 2 cm, and the nonlinear wall temperature profile in Fig. 9 are set, the corresponding nonlinear wall temperature profile with T_s = 612.5 K and T_c = 576.0 K is obtained like Fig. 10. The source region is positioned at x = +5 cm, and the crystal is at x = −5 cm. Fig. 11 shows the axial distribution of partial pressure of component A at the walls resulting from diffusive-convective transport at $g_y = 1g_0$, and equilibrium vapor pressure for Ar = 5 and the nonlinear wall temperature profile of Fig. 9. For the transport path ranged from axial position x = 0 throughout near x = 5, the equilibrium vapor pressures are above the vapor partial pressures of component A, i.e. an undersaturation state, and since at x = 5, the supersaturation along the path occurs. Thus, for our system under consideration in this investigation, the problem of the supersaturation inevitably occur. Fig. 11 is based on Ar = 5, D_{AB} = 0.49 cm^2s^{-1}, P_B = 10 Torr, $g_y = 1g_0$, Pr = 0.82, Le = 0.33, $Gr_t = 2.65 \times 10^4$, $Gr_s = 2.99 \times 10^5$, Pe = 3.74, C_v = 1.02. Fig. 12 shows the axial distribution of partial pressure of component A at the walls in the same system as in Fig. 9, except for D_{AB} = 0.1 cm^2s^{-1}: based on D_{AB} = 0.1 cm^2s^{-1}, Le = 1.59, $Gr_t = 2.85 \times 10^4$, $Gr_s = 3.05 \times 10^5$, Pe = 2.27, C_v = 1.11. To avoid parasitic nucleation near the crystal region, the temperature near the crystal region should be enhanced as maxima as possible, which requires a temperature profile with a larger hump. If the binary diffusion coefficient, D_{AB} is reduced too much small, the smaller temperature profile is needed in the crystal

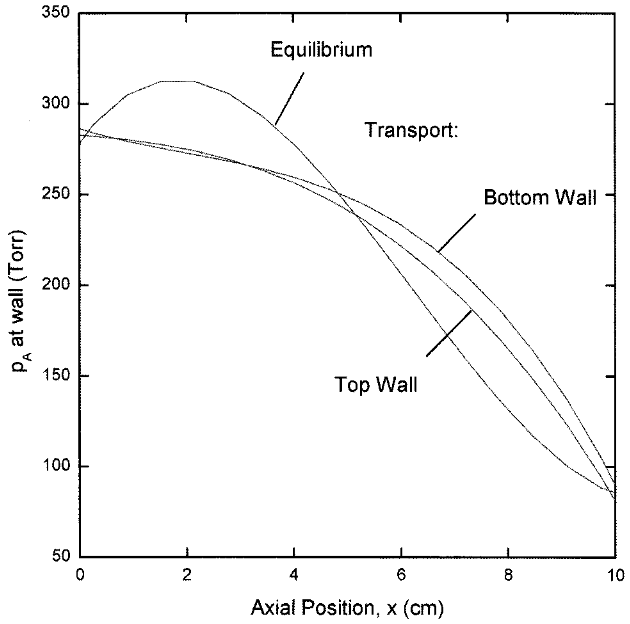

Fig. 11. Axial distribution of partial pressure of component A resulting from diffusive-convective transport and equilibrium vapor pressure at nonlinear wall temperatures. Based on Ar = 5, D_{AB} = 0.49 cm^2s^{-1}, P_B = 10 Torr, $g_y = 1g_0$, Pr = 0.82, Le = 0.33, $Gr_t = 2.65 \times 10^4$, $Gr_s = 2.99 \times 10^5$, Pe = 3.74, C_v = 1.02, T_s = 612.5 K, and T_c = 576.0 K.

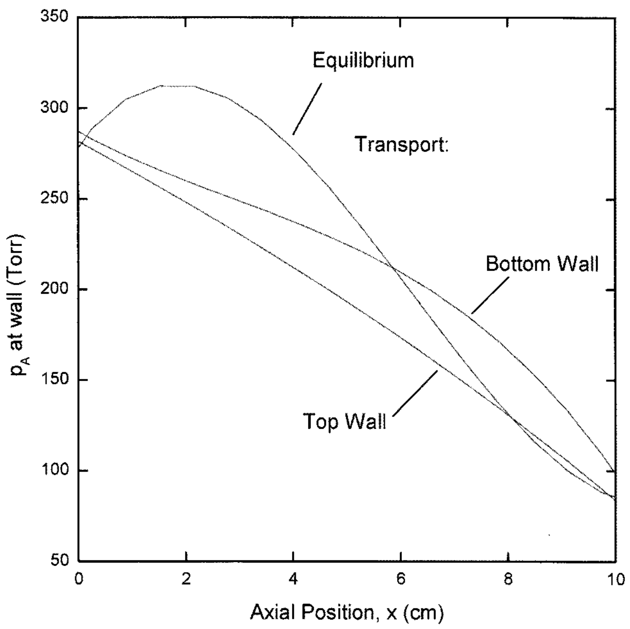

Fig. 12. Axial distribution of partial pressure of component A for the same system as in Fig. 11, except for D_{AB} = 0.1 cm^2s^{-1}. Based on Ar = 5, D_{AB} = 0.1 cm^2s^{-1}, P_B = 10 Torr, $g_y = 1g_0$, Pr = 0.8, Le = 1.59, $Gr_t = 2.85 \times 10^4$, $Gr_s = 3.05 \times 10^5$, Pe = 2.27, C_v = 1.11.

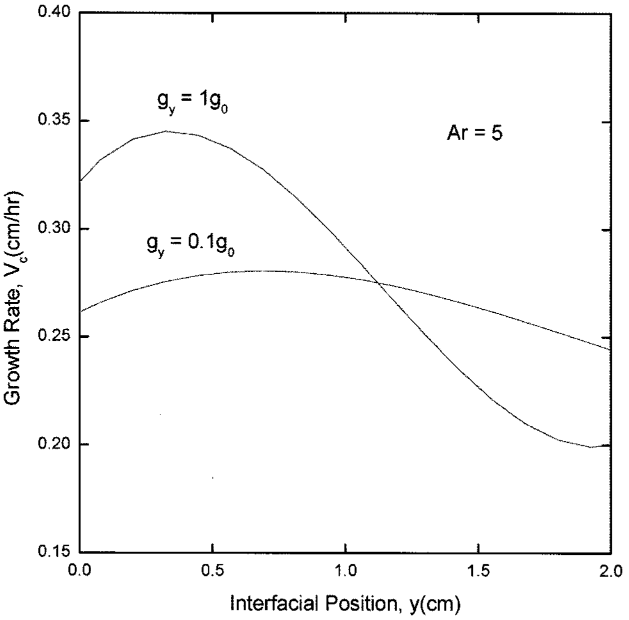

Fig. 13. Interfacial distribution of crystal growth rates for a horizontal ampoule of aspect ratio 5, a nonlinear wall temperature profile between $T_s = 612.5$ K and $T_c = 576.0$ K, and $g_y = 1g_0$ and $0.1g_0$. For the case of $g_y = 1g_0$, the corresponding parameters and operating conditions are $Ar = 5$, $D_{AB} = 0.49\ cm^2s^{-1}$, $Pr = 0.82$, $Le = 0.33$, $Gr_t = 2.65 \times 10^4$, $Gr_s = 2.99 \times 10^5$, $Pe = 3.74$, $C_v = 1.02$.

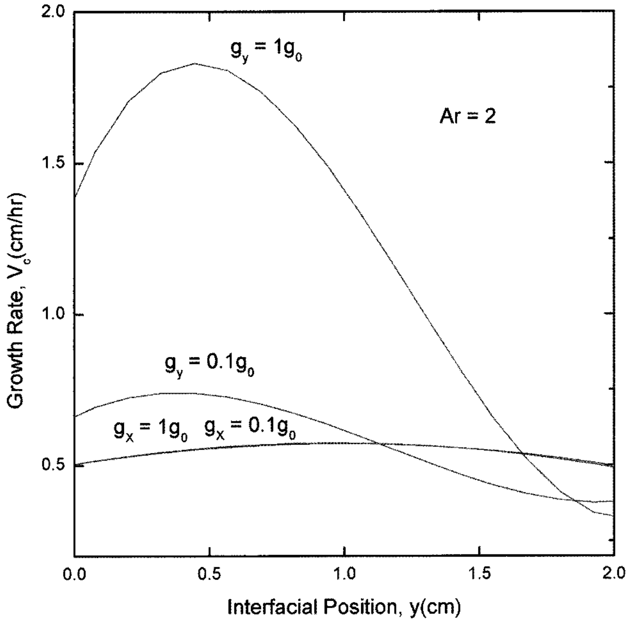

Fig. 14. Interfacial distribution of crystal growth rates for an ampoule of aspect ratio 2, a nonlinear wall temperature profile between $T_s = 615.6$ K and $T_c = 576.0$ K, and $g_y = 1g_0$ and $0.1g_0$. Vertical orientation $g_x = 1g_0$.

region [6]. A reduction of the diffusivity of $0.49\ cm^2s^{-1}$ in Fig. 11 to $0.1\ cm^2s^{-1}$ in Fig. 12 results in a slight shift of supersaturation range into near $x = 6$, and an decrease of at least 20 Torr in partial pressure of Hg_2Cl_2 at the top and bottom walls. It would provide a good insight into the microgravity experiments where the smaller humps would be appropriate to suppress the occurrence of supersaturation along the transport path.

Fig. 13 shows the effects of interfacial distribution of crystal growth rates for a horizontal ampoule of aspect ratio 5, a nonlinear wall temperature profile between $T_s = 612.5$ K and $T_c = 576.0$ K, $g_y = 1g_0$ and $0.1g_0$, $P_B = 10$ Torr. For the case of $g_y = 1g_0$, the corresponding parameters and operating conditions are as follows: $Ar = 5$, $D_{AB} = 0.49\ cm^2s^{-1}$, $P_B = 10$ Torr, $Pr = 0.82$, $Le = 0.33$, $Gr_t = 2.65 \times 10^4$, $Gr_s = 2.99 \times 10^5$, $Pe = 3.74$, $C_v = 1.02$. Fig. 13 are based on the same system as in Fig. 2 except for the nonlinear wall temperature profiles and $P_B = 10$ Torr. In comparison of Fig. 13 with Fig. 2, the profiles of the growth rates for $g_y = 1g_0$ and $0.1g_0$ are the same profile each other, but the magnitudes of the growth rate shown in Fig. 13 are much larger than in Fig. 2 by a factor of 2. This discrepancy is likely to be due to not temperature profiles at walls but the effects of partial pressure of component B, i.e. $P_B = 50$ Torr for Fig. 2 and 10 Torr for Fig. 13. It is reported that when solutal convection is dominated, it is found that the imposed temperature profile has little effect on the growth rate compared with thermal convection [6]. These selections of two different partial pressures of component B are made to avoid oscillatory convection flow fields which result in the problem of convergence of our computer code. Fig. 14 shows the results for a system with an aspect ratio 2 ($L = 4$ cm), $T_s = 612.5$ K and $T_c = 576.0$ K, the gravity accelerations of $g_y = 1g_0$ and $0.1g_0$, $g_x = 1g_0$ and $0.1g_0$. In comparisons of Ar of 2 with 5, the maximum rate for $Ar = 2$ are much greater than for $Ar = 5$ by a factor of 5, but the corresponding nonuniformities in interfacial distributions are also much larger because of the effects of convection. Like the case of Fig. 5, the increase in gravitational level from $g_y = .1g_0$ to 1g in the horizontal orientation position enhances the convection significantly. In comparisons of Fig. 14 with 5, it is found that the maximum growth rates are nearly invariant at $g_y = 1g_0$ at the aspect ratio of 2, except for the partial pressures of component B and temperature profiles at walls. Also, the same trend is obtained for $g_y = 0.1g_0$ and $Ar = 2$. For $Ar = 5$ and $P_B = 10$ Torr, the maximum growth rate for the nonlinear wall temperatures, $0.34\ cmhr^{-1}$ in Fig. 13 is found to be greater than that for the linear wall temperatures, $0.21\ cmhr^{-1}$ (not shown in figures) by a factor of 1.6, which is likely to be due to the thermal boundary conditions imposed under consideration. Note for the cases of $Ar = 5$, increasing the partial pressure of component, B from 10 Torr to 50 Torr results in decreasing the corresponding maximum rate from 0.21 $cmhr^{-1}$ (not shown in figures) down to 0.18 $cmhr^{-1}$ shown in Fig. 2, which is reflected in solutal convection through the binary diffusion coefficient. For the system of $g_x = 1g_0$ and $0.1g_0$, when the ampoule is positioned in the thermally buoyancy driven convectively destabilizing orientation, the growth rates are nearly invariant with the gravity levels of $1g_0$ and $0.1g_0$ and with the conditions of two temperature profiles at walls and with aspect ratios of Ar = 2 and 5.

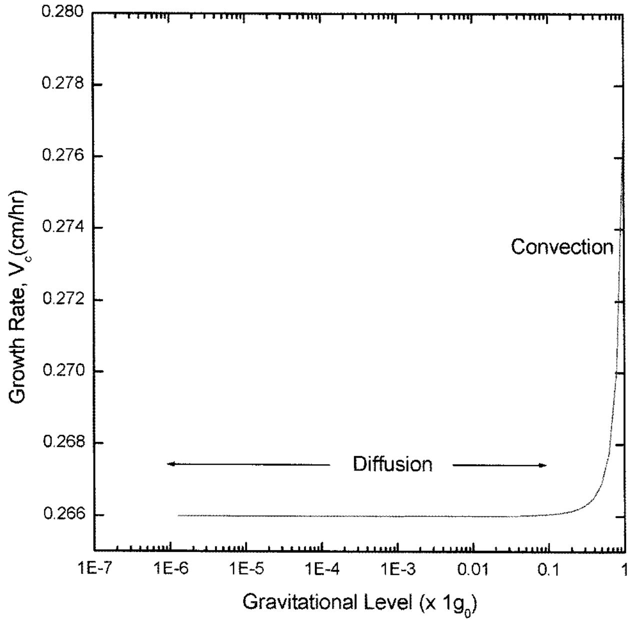

Fig. 15. The effect of the gravitational level on the growth rate of Hg_2Cl_2, for $10^{-6}g_0 \le g \le 1g_0$.

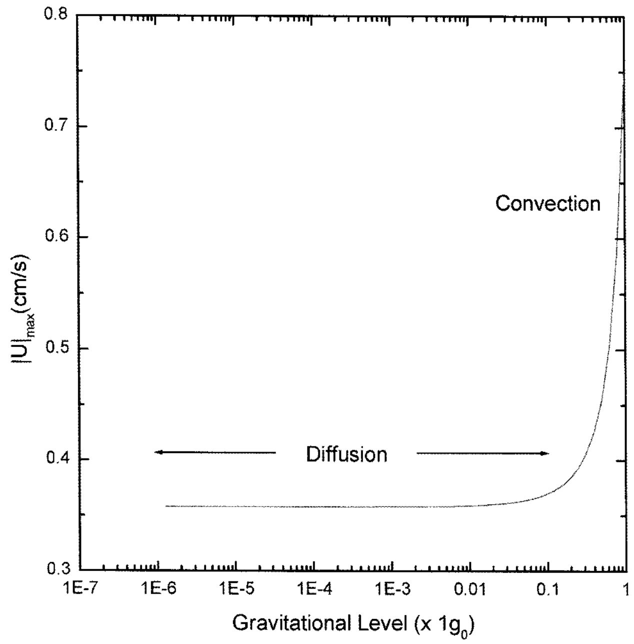

Fig. 16. The effect of the gravitational level on the maximum velocity magnitude, $|U|_{max}$, for $10^{-6}g_0 \le g \le 1g_0$, corresponding to Fig. 15.

Figs. 15 and 16 show the effects of gravitational level on the growth rate of Hg_2Cl_2, and the maximum magnitude of velocity vector, for $10^{-6}g_0 \le g \le 1g_0$, Ar = 5, and nonlinear wall temperatures. As shown in Figs. 15 and 16, the transition from the recirculating convective flow to diffusion-dominated regime occurs near at $g = 0.1g_0$ with tolerable limits. As can be seen in Figs. 3 and 4, the transition appears at $g = 0.1g_0$ and linear wall temperatures.

4. Conclusions

The results of this investigation reveal that, for thermal boundary conditions and reduced gravitational conditions of Hg_2Cl_2-Xe system, the gravity levels have a significant effect on the distribution of growth rate at the crystal interface and convective flow structures. A decrease in aspect ratio from 5 to 2 leads to an increasingly nonuniform interfacial distribution and enhances the growth rate by one-order magnitude for normal gravity and linear wall temperature conditions. The maximum rates under normal and one tenth-reduced gravitational conditions occur in the neighborhood of interfacial position, y = 0.5 cm. It is found that the interfacial growth rate profiles are asymmetrical at y = 1.0 cm. A factor of ten reduction in the gravitational level and an increase in aspect ratio suppress the convective effects on the growth rate. The effect of aspect ratio affects the interfacial growth rates significantly under normal gravity condition rather than under reduced gravitational environments. The transition from the convection-dominated regime to the diffusion-dominated regime ranges near at $0.1g_0$ for both linear wall temperatures and specific nonlinear wall temperatures under consideration in this study. Increasing the molecular weight of component B, Xenon from 2 up to 472, i.e. closer to that of the growing mercurous chloride crystals, results in a reduction in the effect of solutal convection.

Acknowledgements

This paper has been supported by the 2009 Hannam University Research Fund (March 1, 2009 through February 28, 2010). The corresponding author, Geug-Tae

Kim, would like to thank the Hannam University for support of the current investigations through an one-year professor-yeonguneon program starting from September 1, 2008 at the Department of Materials Science & Engineering, University of Florida at Gainesville, Florida, USA.

Nomenclature

A	component Hg_2Cl_2
B	component Xe
D_{AB}	diffusivity of A and B
e_g	unit vector of gravity acceleration
g_0	standard terrestrial acceleration constant, 980.665 cm/s^2
H	width (cm)
L	transport length (cm)
p	pressure
P_T	total pressure
T	temperature
ΔT	temperature difference between source and crystal, $T_s - T_c$
$\Delta\omega$	mass fraction difference between source and crystal, $\omega_{A,s} - \omega_{A,c}$
x	x-coordinate
y	y-coordinate
u	dimensionless x-component velocity
U_c	characteristic velocity, k/L
$\lvert U\rvert_{max}$	dimensional maximum magnitude of velocity vector ($cm\ s^{-1}$)
v	dimensionless y-component velocity
v_x	x-component velocity
v_y	y-component velocity
V	velocity vector

Dimensionless Governing Parameters

Ar	aspect ratio, L/H
C_v	concentration parameter, $C_v = (1 - \omega_{A,c})/\Delta\omega$
Le	Lewis number, k/D_{AB}
Pe	Peclet number, $U_{adv}L/D_{AB}$
Pr	Prandtl number, ν/κ
Gr_t	thermal Grashof number, $g\beta\Delta TH^3/\nu^2$
Gr_s	solutal Grashof number, $g\beta\Delta wH^3/\nu^2$

Subscripts and Superscripts

A	component A, Hg_2Cl_2
B	component B, Xe
c	crystal
H	horizontal
s	source
T	total vapor pressure
*	dimensionless

Greek Letters

β	thermal volume expansion
κ	thermal diffusivity
ν	kinematic viscosity
∇^*	$(\partial/\partial x^*) + (\partial/\partial y^*)$
∇^{*2}	$(\partial^2/\partial x^{*2}) + (\partial^2/\partial y^{*2})$
ϕ	variable (u, v, T^*, ω_A^*)
ψ	dimensionless streamline
ω	mass fraction meaning dimensionless mass concentration density of fluid with component A and B

References

[1] D.W. Greenwell, B.L. Markham and F. Rosenberger, "Numerical modeling of diffusive physical vapor transport in cylindrical ampoules", J. Crystal Growth 51 (1981) 413.

[2] B.L. Markham, D.W. Greenwell and F. Rosenberger, "Numerical modeling of diffusive-convective physical vapor transport in cylindrical vertical ampoules", *J.* Crystal Growth 51 (1981) 426.

[3] B.S. Jhaveri and F. Rosenberger, "Expansive convection in vapor transport across horizontal enclosures", *J.* Crystal Growth 57 (1982) 57.

[4] B.L. Markham and F. Rosenberger, "Diffusive-convective vapor transport across horizontal and inclined rectangular enclosures", J. Crystal Growth 67 (1984) 241.

[5] G.P. Extremet, P. Bontoux and B. Roux, "Effect of temperature gradient locally applied on a long horizontal cavity", Int'l J. Heat and Fluid Flow 8 (1987) 26.

[6] A. Nadarajah, F. Rosenberger and J. Alexander, "Effects of buoyancy-driven flow and thermal boundary conditions on physical vapor transport", J. Crystal Growth 118 (1992) 49.

[7] H. Zhou, A. Zebib, S. Trivedi and W.M.B. Duval, "Physical vapor transport of zinc-telluride by dissociative sublimation", J. Crystal Growth 167 (1996) 534.

[8] F. Rosenberger, J. Ouazzani, I. Viohl and N. Buchan, "Physical vapor transport revised", J. Crystal Growth 171 (1997) 270.

[9] N. Ramachandran, C.H. Su and S.L. Lehoczky, "Modeling studies of PVT growth of ZnSe: current status and future course", J. Crystal Growth 208 (2000) 269.

[10] C. Mennetrier and W.M.B. Duval, "Thermal-solutal convection with conduction effects inside a rectangular enclosure", NASA Technical Memorandum 105371 (1991).

[11] C. Mennetrier, W.M.B. Duval and N.B. Singh, "Physical vapor transport of mercurous chloride under a non-

linear thermal profile", NASA Technical Memorandum 105920 (1992).

[12] J. Lu, Z.-B. Zhang and Q.-S. Chen, "Numerical simulation of the flow field and concentration distribution in the bulk growth of silicon carbide crystals", J. Crystal Growth 292 (2006) 519.

[13] H. Wiedemeier and W. Palosz, "Vapor transport and crystal growth of GeSe under normal and high acceleration", J. Crystal Growth 119 (1992) 79.

[14] Edward R. Letts, James S. Speck and Shuji Nakamura, "Effect of indium on the physical vapor transport growth of AlN", J. Crystal Growth 311 (2009) 1060.

[15] D. Zhuang, Z.G. Herro, R. Schlesser and Z. Sitar, "Seeded growth of AlN single crystals by physical vapor transport", J. Crystal Growth 287 (2006) 372.

[16] J.-S. Kim, Sudhir B. Trivedi, Jolanta Soos, Neelam Gupta and Witold Palosz, "Growth of Hg_2Cl_2 and Hg_2Br_2 single crystals by physical vapor transport", *J. Crystal Growth* 310 (2008) 2457.

[17] N.B. Singh, W.M.B. Duval, A.S.W. Thomas, M.E. Glicksman, J.D. Adam, H. Zhang, J.C. Goldmbeck, C. Watson, R. Naumman, A.E. Nelson, C. Cacioppo, J. Griffin, M. Jugrav, T. Rolin, J. Seaquist and N. Daniel, "Microgravity experiment to understand the effect of convection on PVT crystal growth", Adv. Space Res. 32 (2003) 211.

[18] Ching-Hua Su, S. Feth and S.L. Lehoczky, "In situ partial pressure measurements and visual observation during crystal growth of ZnSe by seeded physical vapor transport", J. Crystal Growth 209 (2000) 687.

[19] Ching-Hua Su, M.A. George, W. Palosz, S. Feth and S.L. Lehoczky, "Contactless growth of ZnSe single crystals by physical vapor transport", J. Crystal Growth 213 (2000) 267.

[20] W. Palosz, "Physical vapor transport of lead telluride", J. Crystal Growth 216 (2000) 273.

[21] W.M.B. Duval, "Convection in the physical vapor transport process--I: Thermal convection", J. Chem. Vapor Deposition 2 (1994a) 188.

[22] W.M.B. Duval, "Convection in the physical vapor transport process--II: Thermosolutal convection", J. Chem. Vapor Deposition 2 (1994b) 282.

[23] W.M.B. Duval, "Transition to chaos in the physical vapor transport process--I: fluid mechanics problem phenomena in microgravity", Fluids Eng. Div. ASME 175 (1993) 51.

[24] W.M.B. Duval, N.E. Glicksman and B. Singh, "Physical vapor transport of mercurous chloride crystals; design of a microgravity experiment", J. Crystal Growth 174 (1997) 120.

[25] P.A. Tebbe, S.K. Loyalka and W.M.B. Duval, "Finite element modeling of asymmetric and transient flow flieds during physical vapor transport", Finite Elements in Analysis and Design 40 (2004) 1499.

[26] G.T. Kim, W.M.B. Duval, N.B. Singh and M.E. Glicksman "Thermal convective effects on physcial vapor transport growth of mercurous chloride crystals (Hg_2C1_2) for axisymmetric 2-D cylindrical enclosure", Modelling. Simul. Mater. Sci. Eng. 3 (1995) 331.

[27] G.T. Kim, W.M.B. Duval and M.E. Glicksman "Thermal convection in physical vapour transport of mercurous chloride (Hg_2Cl_2) for rectangular enclosures", Modelling. Simul. Mater. Sci. Eng. 5 (1997) 289.

[28] G.T. Kim, W.M.B. Duval and M.E. Glicksman "Effects of asymmetric temperature profiles on thermal convection during physical vapor transport of Hg_2Cl_2", Chem. Eng. Comm. 162 (1997) 45.

[29] J.-G. Choi, K.-H. Lee, M.-H. Kwon and G.-T. Kim, "Effect of accelerational perturbations on physical vapor transport crystal growth under microgravity environments", J. Korean Crystal Growth and Crystal Technology 16 (2006) 203.

[30] G.-T. Kim and K.-H. Lee, "Parametric studies on convection during the physical vapor transport of mercurous chloride (Hg_2Cl_2)", J. Korean Crystal Growth and Crystal Technology 14 (2004) 281.

[31] G.T. Kim, "Convective-diffusive transport in mercurous chloride (Hg_2Cl_2) crystal growth", J. Ceramic Processing Research 6 (2005) 110.

[32] J.-G. Choi, K.-H. Lee and G.-T. Kim, "Effects of inert gas (Ne) on thermal convection of mercurous chloride system of Hg_2Cl_2 and Ne during physical vapor transport, J. Korean Crystal Growth and Crystal Technology 18 (2008) 225.

[33] J.-G. Choi, K.-H. Lee and G.-T. Kim, "Generic studies on thermo-solutal convection of mercurous chloride system of Hg_2Cl_2 and Ne during physical vapor transport", J. Korean Crystal Growth and Crystal Technology 1 (2009) 39.

[34] N.B. Singh, R. Mazelsky and M.E. Glicksman, "Evaluation of transport conditions during PVT: mercurous chloride system", PhysicoChemical Hydrodynamics 11 (1989) 41.

[35] N.B. Singh, M. Gottlieb, G.B. Brandt, A.M. Stewart, R. Mazelsky and M.E. Glicksman, "Growth and characterization of mercurous halide crystals:mercurous bromide system", J. Crystal Growth 137 (1994) 155.

[36] N.B. Singh, R.H. Hopkins, R. Mazelsky and J.J. Conroy, "Purification and growth of mercurous chloride single crystals", J. Crystal Growth 75 (1970) 173.

[37] S.J. Yosim and S.W. Mayer, "The mercury-mercuric chloride system", J. Phys. Chem. 60 (1960) 909.

[38] F. Rosenberger and G. Müller, "Interfacial transport in crystal growth, a parameter comparison of convective effects", J. Crystal Growth 65 (1983) 91.

[39] R.B. Bird, W.E. Stewart and E.N. Lightfoot, Transport Phenomena (John Wiley and Sons, New York, NY, 1960).

[40] S.V. Patankar, Numerical Heat Transfer and Fluid Flow (Hemisphere Publishing Corp., Washington D.C., 1980).

[41] D.W. Mackowski, V.R. Rao, D.G. Walker and R.W. Knight, "Numerical investigation of the effects of thermal creep in physical vapor transport", J. Crystal Growth 179 (1997) 297.

[42] I. Catton and D.K. Edwards, "Effects of side walls on natural convection between horizontal plates heated from below", J. Heat Transfer 89 (1967) 259.

[43] D.K. Edwards, "Suppression of cellular convection by lateral walls", J. Heat Transfer 91 (1972) 145.

[42] S.V. Patankar, Numerical Heat Transfer and Fluid Flow (Hemisphere Publishing Corp., Washington D.C., 1980).